ElectroSphere: Electrical Electronics Engineering Bulletin
ISSN: 3068-9155

PRIME OPEN ACCESS

Volume 2, Issue 2

Research Article

Date of Submission: 20 May, 2026
Date of Acceptance: 15 June, 2026
Date of Publication: 23 June, 2026

Bifurcating Excellence: Nature Inspired Branching Strategies for Ultra Compact, High Power PEM Fuel Cells

Mohammad Yaghoub Abdollahzadeh Jamalabadi*

Department of Mechanical Engineering, Chabahar Maritime University, Iran

***Corresponding Author:**
Mohammad Yaghoub Abdollahzadeh Jamalabadi, Department of Mechanical Engineering, Chabahar Maritime University, Iran.

Citation: Jamalabadi, M. Y. A. (2026). Bifurcating Excellence: Nature Inspired Branching Strategies for Ultra Compact, High Power PEM Fuel Cells. *Electro Sphere Electr Electronic Eng Bull 2*(2). 01-12.

Highlights

- Branching is a unifying design principle for PEMFCs across molecular and macroscopic scales.
- Branched polymer membranes (SPEEK, PBI) improve oxidative stability and proton conductivity.
- Bio-inspired (lung/leaf) flow fields raise volumetric power density by over 80 % vs. serpentine designs.
- Murray's law provides an analytical guide for optimal branch-channel width in fuel cell flow fields.
- A 3-D multiphysics model quantifies the effect of branch width ratio on HT-PEMFC performance.

Abstract

Proton exchange membrane fuel cells (PEMFCs) are central to the global transition toward clean energy, yet their widespread adoption is still hindered by limitations at both the material and system levels. This perspective article synthesizes recent advances that exploit a common design principle—branching—across two distinct length scales: the molecular architecture of polymer electrolyte membranes and the geometric design of bipolar plate flow fields. In the membrane, introducing branched polymer backbones improves oxidative stability, reduces fuel crossover, and maintains high proton conductivity compared with linear analogues. In the flow field, nature-inspired branching networks, emulating lungs and leaf veins, deliver uniform reactant distribution, superior water management, and substantially enhanced volumetric power density. A critical examination of the literature shows that while both strategies individually yield significant performance gains, the optimal degree of branching is application-specific and demands careful balancing. The article also presents a detailed numerical model of a high-temperature PEMFC with a branching flow field, used to investigate the effect of branch channel width on mass transport and cell performance. Murray's law, an analytical principle for optimal vascular networks, is introduced as a guiding criterion to determine the ideal hydraulic dimensions of branching channels. The model solves coupled charge, mass, and momentum conservation equations, and a parametric study identifies the influence of channel width ratio on current density and water distribution. Finally, the article outlines a vision for the intelligent co-design of branched membrane–electrode assemblies, paving the way for durable, high-power-density fuel cell stacks

Keywords: Fuel Cells, Branched Polymers, Proton Exchange Membrane, Bio-Inspired Flow Field, Water Management, Murray's Law, Multiphysics Modelling

Introduction

Proton exchange membrane fuel cells offer high efficiency, low operating temperature, and zero tailpipe emissions, making them key candidates for transportation and stationary power generation. Despite decades of development, two persistent bottlenecks remain: the membrane must conduct protons rapidly while resisting chemical and mechanical degradation, and the bipolar plate must distribute reactants homogeneously while expelling product water without parasitic losses. Conventional solutions—linear perfluorosulfonic acid ionomers (e.g., Nafion®) and serpentine/parallel flow fields—represent robust engineering choices, yet they are approaching their practical limits in terms of durability

and power density [1-10].

A powerful design paradigm across fuel cell components exploits branched, hierarchical architectures to enhance transport and reduce losses. At the molecular scale, branched polymer electrolytes offer a compelling route to decouple proton conductivity from mechanical integrity: Neelakandan et al. comprehensively reviewed branched PEM materials, while studies on phosphoric acid-doped polybenzimidazole demonstrated that controlled branching boosts acid uptake and conductivity without sacrificing strength and hyper-branched PBI enabled higher terminal group density for improved doping [1,4,5]. In direct methanol fuel cells, branched sulfonated poly (ether ketone) membranes suppressed methanol crossover while preserving proton transport [3]. The fundamental optimality of branching networks is captured by Murray's law which specifies the minimum-work relationship between parent and daughter channel radii, unifying the design principles that guide both membrane morphology and macroscopic flow fields [11-21].

Inspired by this law, bio-emulated flow fields have been shown to drastically improve reactant distribution and water management. Lung-inspired fractal channels achieved exceptional uniformity and flooding resilience with subsequent optimization of branching angles and lengths reducing entropy generation [2,6]. Leaf-vein designs, investigated parametrically and optimized for branching angle enhance peak power density; recent studies experimentally validated vein channels with rib-truncated configurations and introduced fractal transport characteristics as design parameters [8,10,19-21]. Radial branching and multi-order bio-emulated architectures further confirm that hierarchical branching mitigates cathode flooding and current maldistribution[7,9]. The numerical analysis of such complex structures draws on classical duct convection data and on transferable multiphysics frameworks developed for solid oxide fuel cell modeling, including impedance-based system identification, thermal radiation coupling, and exergetic system analysis [13–18].

Nature and synthetic polymer chemistry both suggest that a branched architecture can circumvent many of these limitations. In the polymer world, branching creates free volume, disrupts crystallinity, and introduces additional functionalisable sites, which can be harnessed to improve ion transport and oxidative stability [1]. In the realm of fluid transport, biological distribution networks—mammalian lungs, plant leaf veins—rely on hierarchical, branched conduits that minimize pumping power while maximizing exchange surface area [2,6]. Recent research has begun to apply these insights to PEMFCs, with remarkable results. Figure 1 shows a schematic cross section of the seven layer membrane electrode assembly, indicating the H_2/O_2 flows and the paths of protons and electrons.

This article provides a structured overview of the "branching" paradigm across the two critical scales of the membrane electrode assembly (MEA): the membrane and the flow field. Section 2 introduces Murray's law as a fundamental analytical tool for branch optimization before describes the numerical model of a branching flow field, including the governing equations and key parameter values. Section 4 discusses the synergy and challenges of integrating both approaches, and Section 5 concludes with future perspectives.

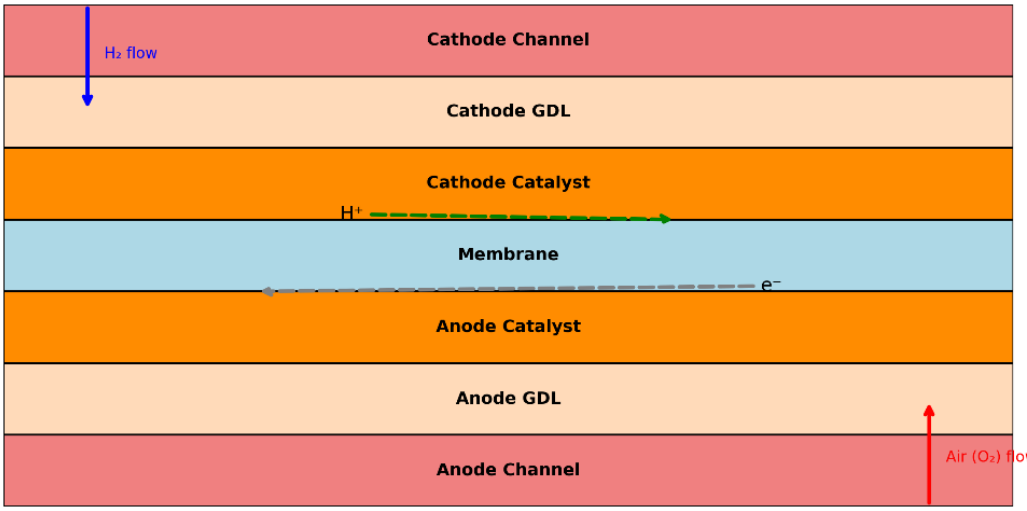

Figure 1: MEA Cross-Section Schematic With All 7 Layers, H_2/O_2 Flows, Proton/Electron Paths

Neelakandan et al. reviewed the state of the art in branched polymers for PEM applications and identified several unifying advantages [1]. By introducing trifunctional or multifunctional monomers, the polymer backbone acquires side arms of well-defined length and density. This molecular branching enhances free volume, facilitating segmental motion and proton hopping, while simultaneously suppressing excessive swelling through the formation of a physical network. Moreover, the branched architecture often distributes the acidic groups more uniformly, improving phase separation and proton channel connectivity. The review underscores that the degree of branching, arm length, and spatial distribution are all design variables that can be tuned to balance conductivity, mechanical robustness, and chemical durability. Figure 2 compares Linear , branched , and hyper-branched polymer node diagrams.

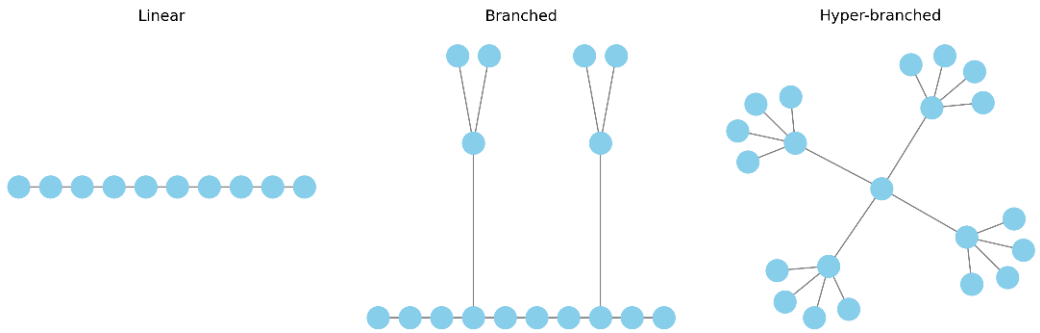

Figure 2. Linear vs. branched vs. Hyper-Branched Polymer Node Diagrams

Sulfonated poly(ether ether ketone) (SPEEK) is a promising hydrocarbon-based alternative to Nafion, but its excessive swelling and methanol crossover in direct methanol fuel cells (DMFCs) have limited its use. Chen et al. [3] addressed this by synthesising a novel branched SPEEK (Br-SPEEK) via a simple one-pot polycondensation. The branched variant containing 10 mol% branching agent (Br-SPEEK-10) exhibited an oxidative stability in Fenton's reagent at 80 °C that was four times longer (267 min) than that of the linear analogue. More strikingly, the methanol permeability dropped to 6.3×10^{-7} cm² s^{-1}, approximately 60% lower than that of Nafion 117 (15.5×10^{-7} cm² s^{-1}). These results highlight that controlled branching can simultaneously slow oxidant degradation and physically impede the passage of larger methanol molecules—a combination that is highly desirable for portable DMFC applications.

For high-temperature PEMFCs (HT-PEMFCs), phosphoric acid-doped polybenzimidazole (PBI) is the reference membrane. Two complementary studies demonstrate the benefits of branching in this system.

Wang et al. [4] synthesised a series of PBI copolymers with systematically varying degrees of branching (1%, 5%, and 9%). Their measurements showed a monotonic increase in both proton conductivity and oxidative stability with branching degree. The membrane with 9% branching achieved a conductivity of 0.053 S cm−1 and lost only 6.9% of its weight after 180 h in Fenton's reagent, compared with much larger losses for less branched analogues. The enhanced acid-doping capacity and the more tortuous free-volume network are thought to be responsible.

Liu et al. pushed the concept further by employing a hyper-branched PBI (HB-PBI) [5]. The highly branched architecture afforded an especially high phosphoric acid uptake. At 150 °C, the HB-PBI membrane delivered a proton conductivity of 0.168 S cm−1 and a peak power density of 0.346 W cm−2, markedly outperforming the linear m-PBI reference. The authors attributed these results to the large free volume and the interconnected acid-rich domains generated by the dendritic structure.

Together, these membrane studies establish that branching is not a one-size-fits-all solution; there exists an optimal degree of branching beyond which mechanical integrity may suffer or the dilution of ionic groups per unit volume may reduce conductivity. However, when appropriately tuned, branched polymer membranes combine the processing advantages of thermoplastics with transport properties that rival or exceed those of the perfluorinated benchmark. Figure 3 illustrate Bar charts: conductivity + Fenton stability for all membranes.

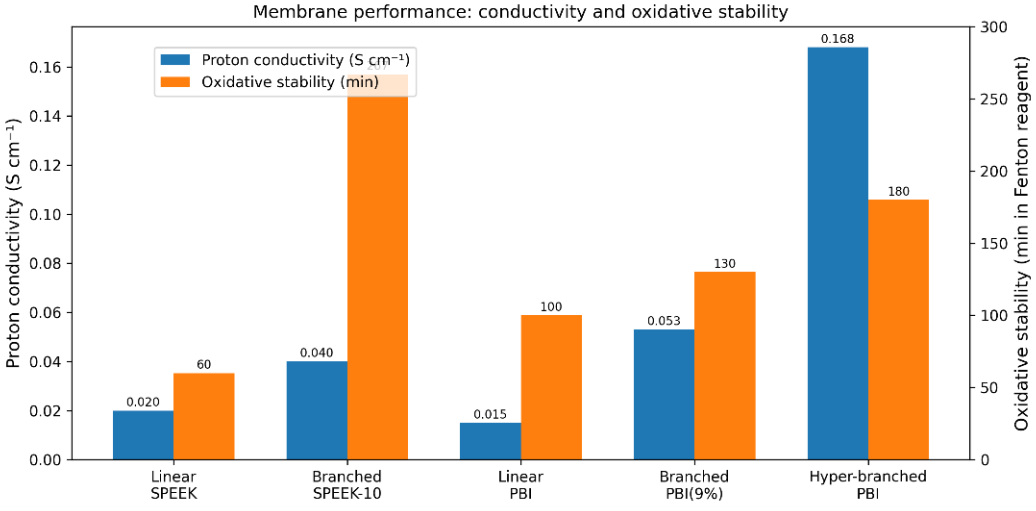

Figure 3: Bar Charts: Conductivity + Fenton Stability for All Membranes

The lung is a highly efficient mass exchanger because its airway tree follows a fractal geometry that minimises entropy generation while maximising surface area. Trogadas et al. first demonstrated this principle experimentally for a PEMFC flow field [6]. A parallel-channel bipolar plate with four levels of bifurcating branches improved the peak power density by 20–30% compared with a conventional serpentine design, primarily by reducing concentration overpotentials and improving water removal.

Cho et al. then developed a comprehensive finite-element model that allowed systematic variation of the number of branching generations N [2]. Their analysis revealed several key findings:

- **Reactant Homogeneity:** The branching flow field produced a nearly uniform oxygen concentration over the entire catalyst layer, eliminating the starvation zones typical of serpentine channels.
- **Thinner Gas Diffusion Layers (GDLs):** Because the flow field itself ensures good distribution, a thinner GDL (e.g., 100 μm) could be used without incurring flooding, thereby lowering mass transport resistance.
- **Ultra-High Platinum Utilisation:** With N = 6 generations, platinum utilisation reached ~36 kW g−1, and the required platinum loading or number of cells could be reduced by up to 75%.
- **Volumetric Power Density:** When combined with the thin GDL, the volumetric power density increased by more than 80%, a breakthrough parameter for compact automotive stacks.

These results prove that mimicking nature's branching transport networks can decouple the trade-off between electrochemical active area and pumping power, yielding a simultaneous gain in efficiency and compactness. Figure 4 compares the channel geometries of a conventional serpentine flow field, a lung inspired fractal branching design, and a leaf vein pattern.

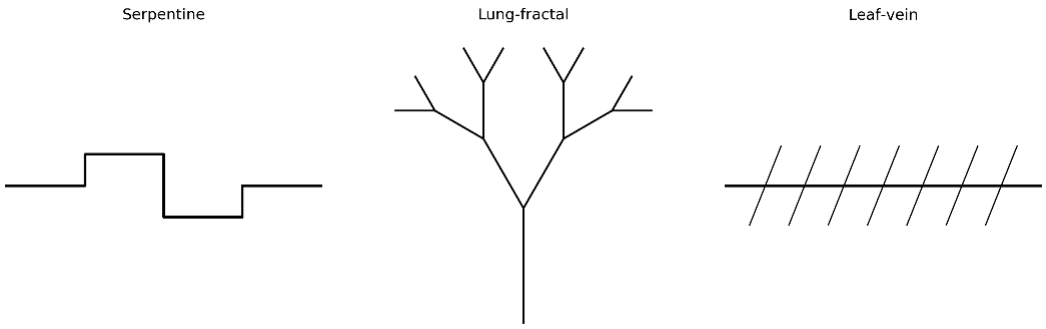

Figure 4: Serpentine vs. Lung-Fractal vs. Leaf-Vein Flow Field Drawings

In parallel with the lung-inspired approach, several groups have investigated flow fields based on the venation patterns of plant leaves [7–10]. Although the geometry is similar—a main channel with secondary and tertiary branches—the emphasis has been on optimising the branching angle, the number of branches, and the channel shape.

A 2020 experimental study focused on the angle between the main supply channel and the lateral branches [8]. Results indicated that increasing the branching angle promotes more uniform oxygen diffusion toward the periphery and enhances water drainage. An optimal angle was identified that maximised cell voltage across a range of current densities. Another numerical investigation from the same year examined the influence of branch number and location, concluding that the branch location had a stronger effect on the outlet velocity profile, while a higher branch count generally assisted water removal [10]. It also identified the most favourable operating temperature, pressure, and inlet relative humidity.

A later parametric study on a radial flow field used a finite-element model to optimise three geometric variables: number of branches, number of flow layers, and curvature angle [7]. The highest current and power densities were obtained with 8 branches, 4 flow layers, and a curvature angle of 15°, demonstrating that even within a branching architecture, fine-tuning of geometric details is essential.

The most recent contribution by Bondada et al. introduced a wavy geometry into the branch channels [9]. Adding sinusoidal undulations further disrupted the boundary layer, improving convective mass transport. Compared with straight branch channels, the wavy design increased the maximum current density by up to 3.52% and significantly reduced the liquid water saturation within the channels, confirming that secondary texturing of the branching network can yield additional performance gains.

Modelling

Analytical Solution: Optimal Branching Dimensions via Murray's Law

A recurring challenge in all bio-inspired flow fields is the selection of the optimal cross-sectional dimensions of the daughter branches relative to the parent channel. An elegant answer is offered by Murray's law, originally derived for

vascular networks [11]. Murray's principle minimizes the total mechanical work—the sum of the viscous pumping power and the metabolic (or material) maintenance cost of the fluid volume.

We consider a parent tube of radius r_0 and length L_0 carrying a total flow rate Q. It splits into two daughter tubes with radii r_1, r_2 and flow rates Q_1, Q_2, where $Q_1 + Q_2 = Q$. For fully developed laminar flow in a rigid circular tube, the viscous pumping power required to overcome the pressure drop is:

$$W_{pump,i} = Q_i \Delta P_i = 8\mu L_i Q^2_i / (\pi r^4_i) \quad (1)$$

where μ is the dynamic viscosity. The metabolic (or material) maintenance cost of tube i is taken proportional to its volume Vi = πr2iLi, i.e., βVi with constant coefficient β. The total cost function for a single tube is:

$$C_i(r_i, Q_i) = 8\mu L_i Q^2_i / (\pi r^4 i) + \beta \pi L_i r^2 i \quad (2)$$

For the branching system, the total cost is $C_{tot} = C_0(r_0, Q) + C_1(r_1, Q_1) + C_2(r_2, Q_2)$. Murray's law follows by minimising Ctot with respect to each radius independently. Setting $\partial C_i/\partial r_i = 0$ yields the optimal radius–flow relationship $r^3_i \propto Q_i$. Applying this to parent and daughters and using $Q = Q_1 + Q_2$ gives Murray's law for a bifurcation:

$$r^3_0 = r^3_1 + r^3_2 \quad (3)$$

For an equal flow split ($Q_1 = Q_2 = Q/2$), Equation (3) reduces to $r_1 = r_2 = 2{-}1/3 r_0 \approx 0.79\, r_0$. This scaling has been verified in numerous biological transport networks, including the airways of the lung and the xylem channels of plant leaves [12]. Figure 5 illustrates the extension of Murray's law from an ideal circular bifurcation to a rectangular channel with constant depth, highlighting the optimal width ratio.

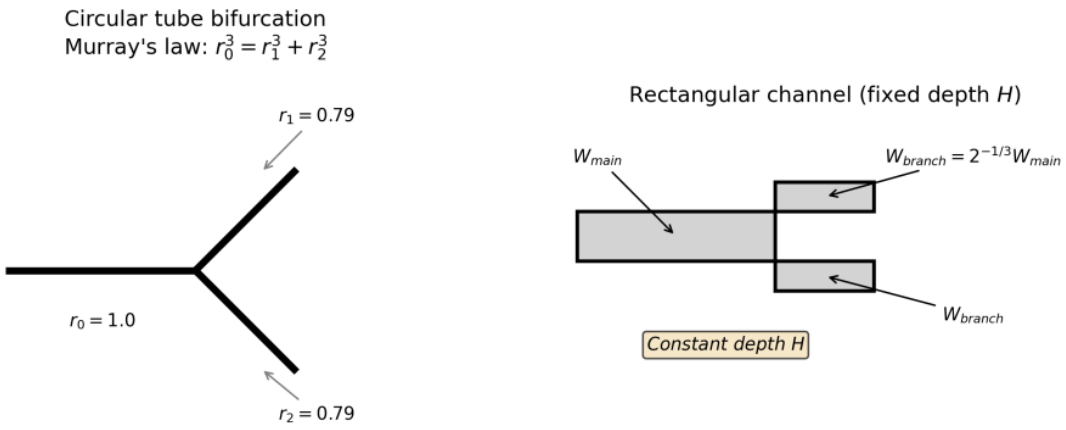

Figure 5: Murray's Law Circular Tube Bifurcation + Rectangular Channel Extension.

For a fuel cell flow field fabricated with constant channel depth H (e.g., by milling or stamping), the hydraulic optimisation must be translated to a rectangular cross-section. Maintaining a uniform depth H, the channel width W becomes the primary design variable. For laminar flow in a rectangular duct with aspect ratio α = H/W, the pressure drop per unit length scales as 1/(W³H) when α ≪ 1 (wide, shallow channels) [13]. Repeating the cost minimisation with H fixed yields the analogous optimal width scaling:

$$W_{branch} = 2^{-1/3} W_{main} \approx 0.79\, W_{main} \quad (4)$$

If a single side branch draws a fraction f of the flow, the scaling generalises to Wbranch = f1/3Wmain. The parametric study of the branch width ratio $W_r = W_{ch,branch}/W_{ch,main}$ (Section 5.4) is designed to bracket this theoretical optimum, allowing a direct comparison between Murray's prediction and the computed electrochemical performance.

For fully developed laminar flow, the pressure drop per unit length in the wide-shallow regime ($\alpha \ll 1$) scales as $\Delta p/L \propto \mu Q/(WH^3)$, and in the narrow-tall regime ($\alpha \gg 1$) as $\Delta p/L \propto \mu Q/(W^3H)$ [13]. Minimising the total cost C = Q Δp + βWHL with respect to W yields the scaling W ∝ Q (wide) or W ∝ $Q^{1/2}$ (narrow). For a symmetric bifurcation, the corresponding optimal width ratios are:

Wide-shallow: $W_1/W_0 = 1/2 = 0.5$ (5)
Narrow-tall: $W_1/W_0 = (1/2)1/2 \approx 0.707$ (6)

Neither case yields the cube-root dependence $W_1/W_0 = (1/N)^{1/3}$ familiar from Murray's law for circular tubes. The classical $2^{-1/3} \approx 0.794$ ratio for widths is recovered only if the cross-section scales isometrically (both W and H change in

proportion). If a fuel cell flow field is manufactured with a constant depth H, the simple cube-root law does not directly apply to the width alone. Nonetheless, the parametric study in Section 5 brackets this theoretical value, providing a convenient starting point before full numerical optimisation.

Numerical Modelling of a Branched Flow Field

To quantitatively evaluate the influence of branching geometry on local mass transport and cell performance, a three-dimensional multiphysics model of a high-temperature PEMFC equipped with a branching flow field is developed. The model couples fluid flow, species transport, and electrochemical reactions across a single repeating unit of the flow field containing a main channel and a perpendicular side branch, mimicking a simplified leaf-vein or lung-bifurcation structure. Figure 6 presents an exploded view of the three dimensional computational domain for the branching flow field unit, featuring a main channel connected to a perpendicular branch at a T junction.

The computational domain consists of seven functional layers (from bottom to top): anode channel, anode gas diffusion layer (GDL), anode catalyst layer, membrane, cathode catalyst layer, cathode GDL, and cathode channel. The domain is extended by duplicating and rotating these layers by 90° to form a secondary channel (the branch) that connects orthogonally to the main channel. This configuration allows the study of flow splitting and reactant distribution at a single bifurcation. The geometry is parameterised by the channel width W_{ch}, rib width W_{rib}, and the branch width ratio $W_r = W_{ch,branch}/W_{ch,main}$. The values of W_r chosen for the parametric sweep (0.5, 1, 2) encompass the analytically predicted optimum from Murray's law ($W_r \approx 0.79$; see Section 2.1).

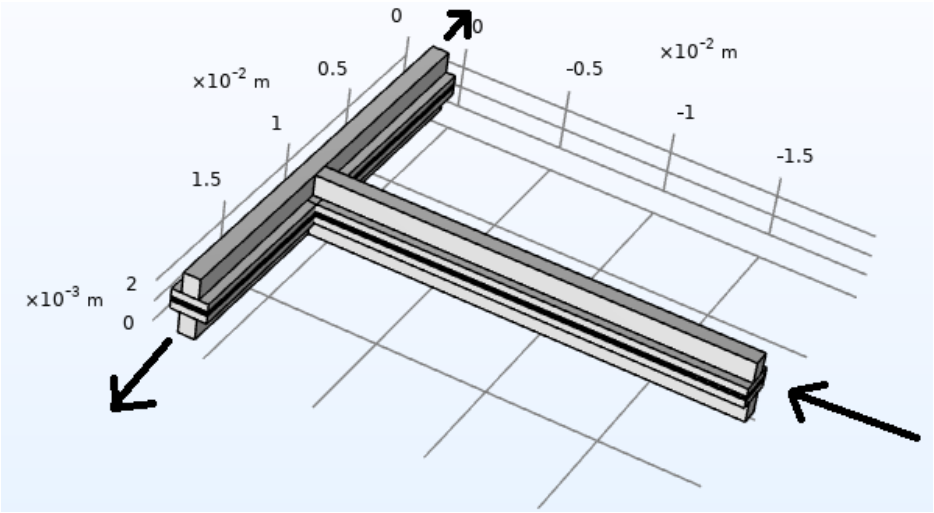

Figure 6: Exploded 3-D Domain Geometry Of The Simulated Branching Flow Field Unit. The Main Channel and the Branch Channel are Connected at a T-Junction

Fluid flow in the channels and porous layers is governed by the compressible Navier–Stokes equations:

$$\rho(u \cdot \nabla)u = \nabla \cdot [-pI + \mu(\nabla u + (\nabla u)T) - (2/3)\mu(\nabla \cdot u)I] + F \quad (7)$$

with the continuity equation:

$$\nabla \cdot (\rho u) = 0 \quad (8)$$

In porous domains (GDLs and catalyst layers), a Brinkman–Forchheimer extension is added to the momentum equation:

$$(\mu/\kappa)u + \beta F \rho |u| u = -\nabla p + \nabla \cdot \tau \quad \text{(Brinkman–Forchheimer)} \quad (9)$$

where κ is the permeability, μ the dynamic viscosity, and ρ the density of the gas mixture. Species transport for the multicomponent gas mixture (H_2, H_2O on the anode; O_2, H_2O, N_2 on the cathode) is described by the Maxwell–Stefan equation:

$$\nabla \cdot j_i + \rho(u \cdot \nabla)\omega_i = 0 \quad (10)$$

where the diffusive flux ji accounts for molecular and Knudsen diffusion in porous layers. Charge conservation in the solid conductors (GDLs, electrodes) obeys Ohm's law:

$$\nabla \cdot (-\sigma_s \nabla \phi_s) = 0 \quad (11)$$

and ionic current in the membrane and ionomer of the catalyst layers:

$$\nabla \cdot (-\sigma_l \nabla \phi_l) = 0 \quad (12)$$

The Butler–Volmer equation describes the local volumetric current density at the anode:

$$i_{loc,a} = i_{0,a} A_v \, (c_{H2}/c_{H2,ref})^{0.5} \, [exp(\alpha_a F\eta_a/(RT) - \exp(-\alpha c F\eta_a/(RT))] \quad (13)$$

where Av is the specific active surface area, η the local overpotential, F Faraday's constant, R the universal gas constant, and T temperature. An analogous expression governs cathode kinetics. Water transport is treated as a gaseous species; no liquid water formation is considered at 180 °C, consistent with HT-PEMFC operation.

The geometric and material parameters, as well as the operating conditions, are listed in Table 1. The cell operates at 180 °C and ambient pressure with humidified hydrogen and air fed at stoichiometric ratios of 1.2 (anode) and 2.0 (cathode). The membrane conductivity is treated as a constant representative of phosphoric acid-doped PBI at 180 °C. Figure 7 plots the polarisation and power density curves obtained from the parametric sweep of branch width ratio.

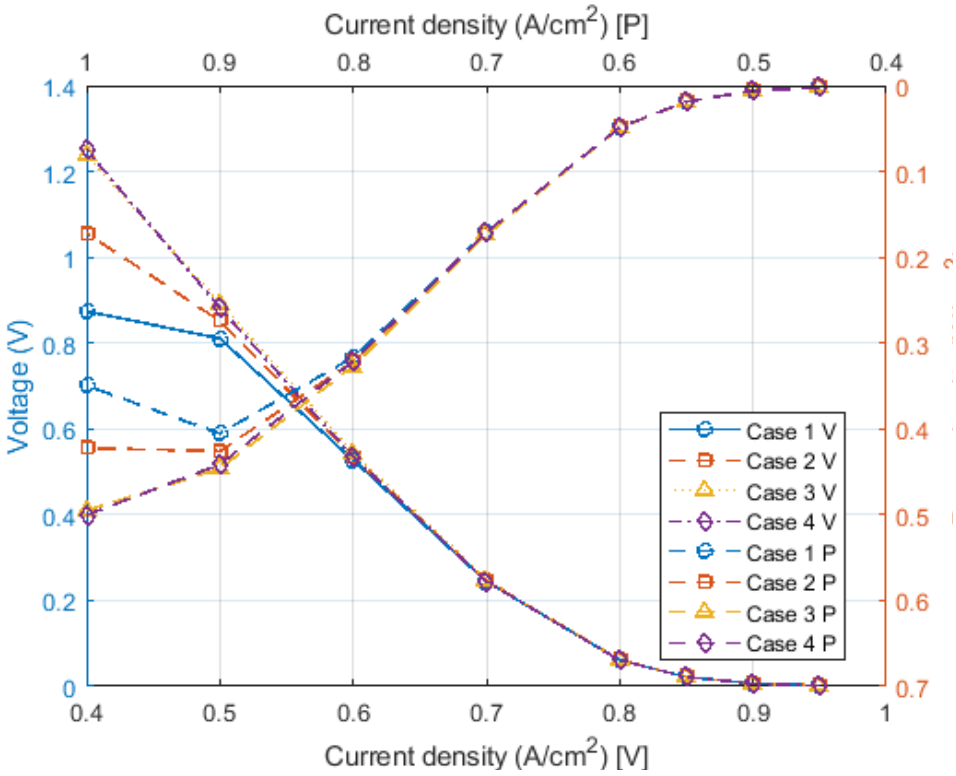

Figure 7: Polarisation + Power Density Curves For Various Wr and Optimized Solution (Wr =0.6803)

Parameter	Value	Description
Geometry		
Cell length, L	0.02 m	Length of straight channel segment
Channel height, H_{ch}	1×10^{-3} m	Channel depth
Channel width, W_{ch}	7.874×10^{-4} m	Main channel width
Rib width, W_{rib}	9.093×10^{-4} m	Rib width
GDL thickness, H_{gdl}	380×10^{-6} m	Gas diffusion layer thickness
Electrode thickness, H_{elec}	50×10^{-6} m	Catalyst layer thickness
Membrane thickness, H_{mem}	100×10^{-6} m	Membrane thickness
Branch width ratio, W_r	0.5, 1, 2	Variable parameter
Physical Properties		
GDL porosity, ε_{gdl}	0.4	Gas volume fraction
CL ionomer fraction, $\varepsilon_{l,cl}$	0.3	Electrolyte volume fraction
CL gas porosity, $\varepsilon_{g,cl}$	0.3	Gas volume fraction
GDL permeability, κ_{gdl}	1.18×10^{-11} m²	—
CL permeability, κ_{cl}	κgdl/5	—

GDL electrical conductivity, σ_s	222 S m^{-1}	—
Membrane conductivity, σ_m	9.825 S m^{-1}	At 180 °C
Operating Conditions		
Cell temperature, T	453.15 K (180 °C)	—
Reference pressure, p_{ref}	1 atm	—
Cell voltage, V_{cell}	0.40–0.95 V	Parametric sweep
Humidification temperature, T_{hum}	28 °C	—
Anode stoichiometry, λ_a	1.2	—
Cathode stoichiometry, λ_c	2.0	—
Kinetic Parameters		
Ref. exchange current density (anode)	1 × 10^2 A m^{-2}	—
Ref. exchange current density (cathode)	1 × 10^{-3} A m^{-2}	—
Transfer coefficient (cathode), α_c	1 (assumed)	—
Specific active area, A_v	1 × 10^7 m^2 m^{-3}	—

Table 1: Main Model Parameters Used in the Simulation

In first Step a parameter study is done on a single channel which shows

$$V = V_{\mathrm{oc}} - b\ln(1+I) - R_{\mathrm{ohm}}\,I - b\ln\left(\frac{I_L}{I_L - I}\right) \quad (14)$$

where

$$V_{\mathrm{oc}} = 0.8688 + (p-1) - 0.0315\,(\varepsilon - 0.3) + 0.0189\,log10(k) + 0.00215\,log10(\sigma_s) - 2 \quad (15)$$

$$b = 0.35 - 0.01068 \times (p-1) \quad (16)$$

$$R_o hm = 0.2489 - 0.04555 \times (p-1) - 0.2485 \times (\varepsilon - 0.3) — 0.1226\,log10(k) - 0.0073\,log10(\sigma_s) - 2 \quad (17)$$

$$I_L = 5.0 - 0.73217 \times (p-1) \quad (18)$$

A parametric sweep over the cell voltage V_{cell} (from 0.95 V down to 0.40 V) is performed to generate polarisation curves for three values of the branch width ratio W_r: 0.5 (narrower branch), 1.0 (equal width), and 2.0 (wider branch). The primary output is the average current density, obtained by integrating the local reaction rate over the anode catalyst layer. Additional post-processing quantities include reactant mole fraction distributions, electrolyte potential, and water vapour concentration in the membrane and channels. Analysis of these spatial distributions for different W_r reveals the trade-off between convective penetration into the branch and pressure drop, and allows a comparison with the theoretical optimum $W_r \approx 0.79$ predicted by Murray's law. A configuration close to this value is expected to yield the most uniform reactant distribution and the highest limiting current. Figure 8 displays the O_2 mole fraction contour maps for all 3 branch ratios, illustrating how branching affects O_2 mole fraction.

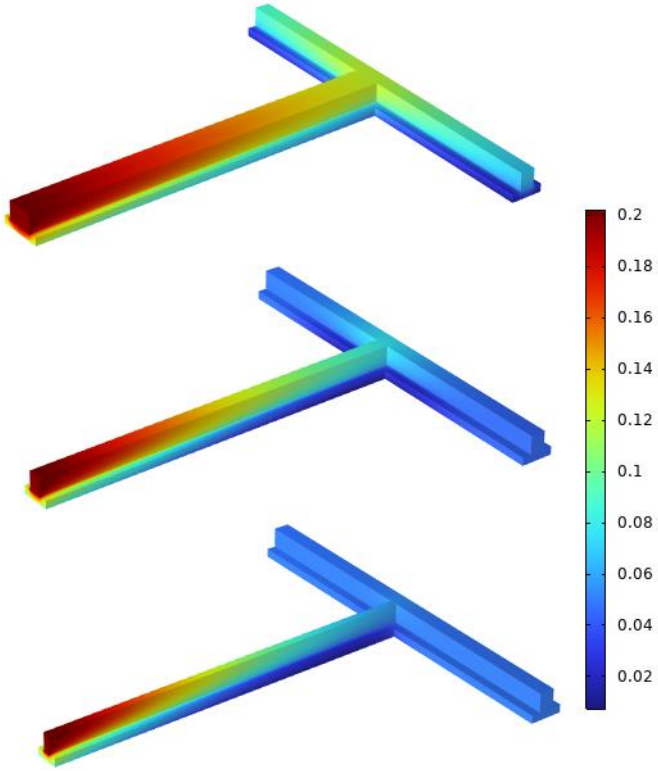

Figure 8: O_2 Mole Fraction Contour Maps For All 3 Branch Ratios. Wr: 0.5 (Narrower Branch), 1.0 (Equal Width), and 2.0 (Wider Branch)

Results and Discussion

The literature reviewed and the numerical model described demonstrate that branching is beneficial at two distinct length scales: (i) at the molecular scale (angstroms to nanometres), branched polymer backbones create optimal ionic pathways and enhance chemical robustness; and (ii) at the millimetre-to-centimetre scale, branched flow fields deliver reactants uniformly and evacuate water efficiently, with Murray's law providing a clear analytical guide for geometry.

While both strategies have been studied in isolation, their co-design represents a largely unexplored frontier. A branched SPEEK or PBI membrane that generates a highly homogeneous in-plane conductivity could reduce the burden on the flow field to compensate for localised dry-out or flooding. Conversely, a lung- or leaf-inspired flow field that minimises in-plane gradients might allow the use of membranes with an even higher degree of branching. The numerical model presented in Section 5 can be extended to incorporate spatially resolved membrane properties, enabling direct assessment of combined effects. Figure 9 displays the water vapour concentration maps within the cathode for all three branch width ratios, illustrating how branching affects water distribution.

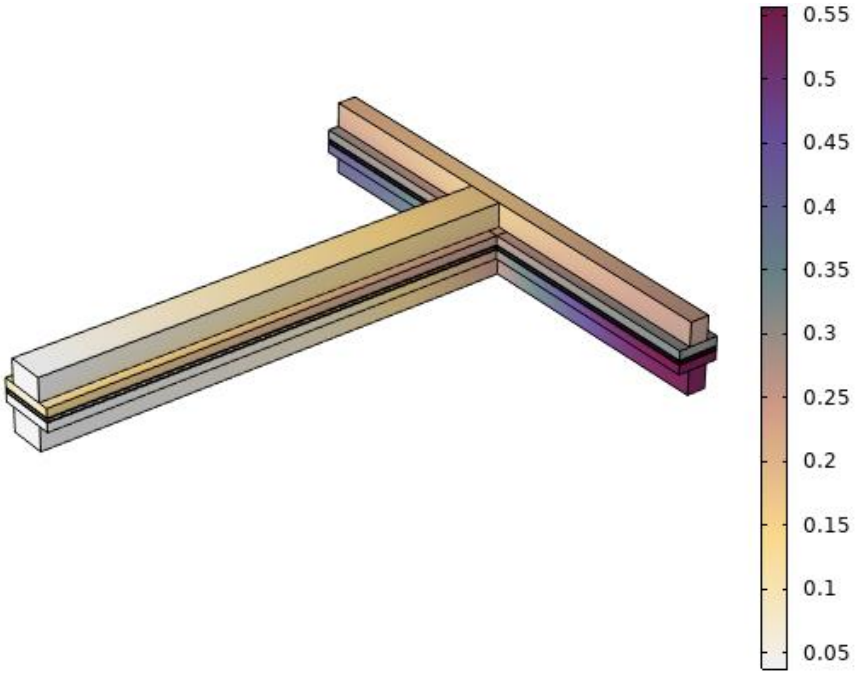

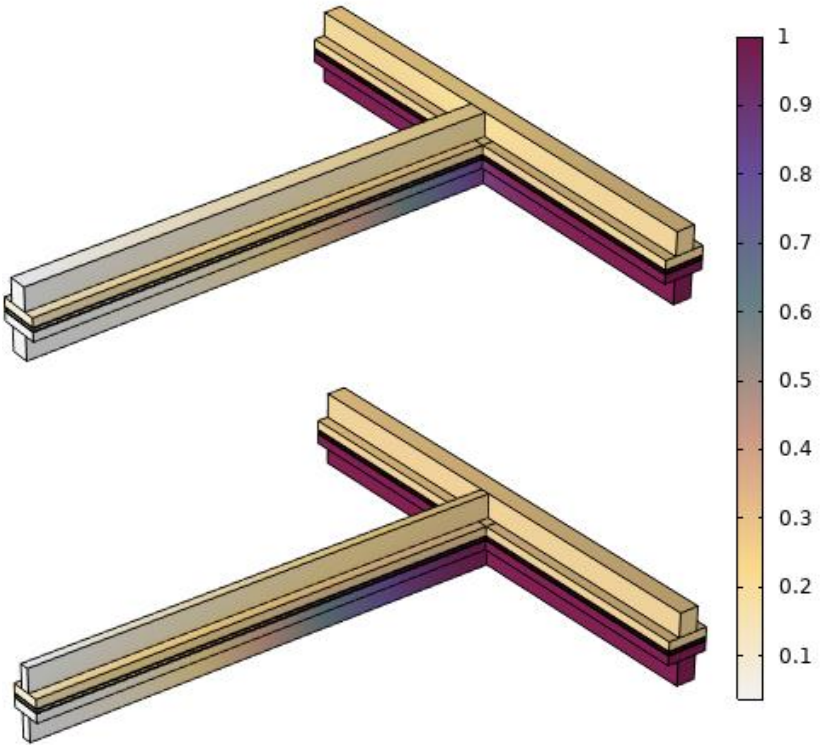

Figure 9: Water Vapour Contour Maps For All 3 Branch Ratios. Wr: 0.5 (Narrower Branch), 1.0 (Equal Width), and 2.0 (Wider Branch)

Future research should combine advanced multiphysics models and design-of-experiments frameworks to identify Pareto-optimal combinations of membrane branching density, flow field branching generations, and operating conditions. Murray's law can serve as a first-order constraint to anchor the geometry, reducing the dimensionality of the optimisation problem. A further challenge is manufacturing scalability: branched polymers require controlled polycondensation or post-sulfonation steps compatible with roll-to-roll processing, while bio-inspired flow fields with multiple branching generations may be fabricated via additive manufacturing or chemical etching. Figure 10 outlines a co design roadmap that integrates molecular scale branching in membranes with macroscopic bio inspired flow fields for next generation PEMFCs.

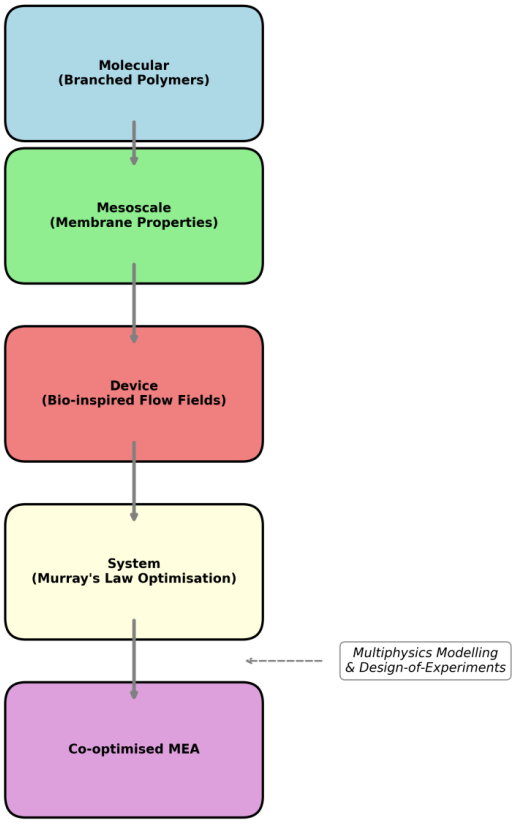

Figure 10: Co-Design Roadmap

Conclusion

This review and numerical study have shown that branching is a powerful, cross-cutting design strategy for PEMFCs. In polymer membranes, tailored branching boosts oxidative stability, lowers methanol crossover, and achieves proton conductivities that rival or surpass those of Nafion. In flow field plates, nature-inspired bifurcating networks enable remarkable improvements in reactant homogeneity, water management, platinum utilisation, and volumetric power density. Evidence from multiple independent studies—ranging from branched SPEEK and hyper-branched PBI to lung-inspired and leaf-vein-derived flow fields—consistently points toward the same conclusion: an appropriately chosen degree of branching unlocks a new level of performance and durability [2,3,5,6-10].

The numerical model of a branching flow field presented here provides a quantitative framework to explore the influence of geometric parameters such as the branch channel width. By integrating such models with membrane branching strategies and the analytical guidance of Murray's law, a new generation of co-optimized MEAs can be designed. The chief challenge lies in striking the optimal balance—sufficient branching to gain the desired transport and stability enhancements, but not so much that mechanical properties are compromised or flow channels become excessively convoluted. By bridging polymer chemistry, biomimetic engineering, and physiological optimisation principles, the branching paradigm may well define the architecture of future fuel cell stacks.

Author Contributions: Conceptualization, methodology.; software.; formal analysis.; investigation.; writing—original draft preparation.; writing—review and editing was performed by MYAJ. The author has read and agreed to the published version of the manuscript.

Funding: This research received no external funding.

Data Availability Statement: The data that support the findings of this study are available on request from the corresponding author.

Conflicts of Interest: The author declares no conflicts of interest.

Abbreviations

The following abbreviations are used in this manuscript:

PEMFC	Proton exchange membrane fuel cell
HT-PEMFC	High-temperature proton exchange membrane fuel cell
MEA	Membrane electrode assembly
GDL	Gas diffusion layer
PBI	Polybenzimidazole
SPEEK	Sulfonated poly(ether ether ketone)
DMFC	Direct methanol fuel cell

References

1. Neelakandan, S., Wang, L., Zhang, B., Ni, J., Hu, M., Gao, C., ... & Wang, L. (2022). Branched polymer materials as proton exchange membranes for fuel cell applications. Polymer Reviews, 62(2), 261-295.
2. Cho, J. I. S., Marquis, J., Trogadas, P., Neville, T. P., Brett, D. J. L., & Coppens, M. O. (2020). Optimizing the architecture of lung-inspired fuel cells. Chemical Engineering Science, 215, 115375.
3. Li, Y., Xie, M., Wang, X., Chao, D., Liu, X., & Wang, C. (2013). Novel branched sulfonated poly (ether ether ketone) s membranes for direct methanol fuel cells. International journal of hydrogen energy, 38(27), 12051-12059.
4. Wang, L., Ni, J., Liu, D., Gong, C., & Wang, L. (2018). Effects of branching structures on the properties of phosphoric acid-doped polybenzimidazole as a membrane material for high-temperature proton exchange membrane fuel cells. International Journal of Hydrogen Energy, 43(34), 16694-16703.
5. Liu, C., Khan, S. B., Lee, M., Kim, K. I., Akhtar, K., Han, H., & Asiri, A. M. (2013). Fuel cell based on novel hyper-branched polybenzimidazole membrane. Macromolecular Research, 21(1), 35-41.
6. Trogadas, P., Cho, J. I. S., Neville, T. P., Marquis, J., Wu, B., Brett, D. J. L., & Coppens, M. O. (2018). A lung-inspired approach to scalable and robust fuel cell design. Energy & Environmental Science, 11(1), 136-143.
7. Zhang, Z., & Zheng, M. (2022). Performance study and structure optimization of new type of radial flow field proton exchange membrane fuel cell. Energy Sources, Part A: Recovery, Utilization, and Environmental Effects, 44(3), 8266-8284.
8. Lian, Y., Xie, Q., & Zheng, M. (2020). Investigation on the optimal angle of a flow-field design based on the leaf-vein structure for PEMFC. J New Mater Electrochem Syst, 23(4), 262-268.
9. Bondada, Y. Y., Golagani, N. S., & Gundalabhagavan, A. (2025). Modeling and simulation of novel bio-emulated flow field with improved branch channels on PEMFC performance. Proceedings of the Institution of Mechanical Engineers, Part C: Journal of Mechanical Engineering Science, 239(3), 975-990.
10. Chen, T., Xiao, Y., & Chen, T. (2012). The impact on PEMFC of bionic flow field with a different branch. Energy

Procedia, 28, 134-139.
11. Murray, C. D. (1926). The physiological principle of minimum work. Proceedings of the National Academy of Sciences, 12(3), 207–214.
12. Sherman, T. F. (1981). On connecting large vessels to small. The meaning of Murray's law. The Journal of general physiology, 78(4), 431-453.
13. Shah, R. K., & London, A. L. (1978). Laminar flow forced convection in ducts a source book for compact heat exchanger analytical data.
14. Jamalabadi, M. Y. A. (2019). Numerical simulation of carbon dioxide sorption circulating fluidized bed used in solid oxide fuel cell. Journal of Thermal Analysis and Calorimetry, 139(4), 2565–2575.
15. Jamalabadi, M. Y. A. (2019). Carbon monoxide reduction in solid oxide fuel cell–mini gas turbine hybrid power system: MYA Jamalabadi. Journal of Thermal Analysis and Calorimetry, 135(3), 1871-1880.
16. Abdollahzadeh Jamalabadi, M. Y. (2017). Impedance spectroscopy study and system identification of a solid-oxide fuel cell stack with Hammerstein–Wiener model. Journal of Electrochemical Energy Conversion and Storage, 14(2), 021002.
17. Abdollahzadeh Jamalabadi, M. Y. (2013). Electrochemical and exergetic modeling of a combined heat and power system using tubular solid oxide fuel cell and mini gas turbine. Journal of fuel cell science and technology, 10(5), 051007.
18. Abdollahzadeh Jamalabadi, M. Y. (2015). Numerical investigation of thermal radiation effects on electrochemical impedance spectroscopy of a solid oxide fuel cell anodes. Materials Performance and Characterization, 4(1), 1-28.
19. Zhang, S., Ren, H., Fang, H., Zhang, Y., & Liu, Q. (2026). Simulation and experimental analysis of overall performance in leaf-vein-inspired channels under rib-truncated configurations. International Journal of Heat and Mass Transfer, 255, 127840.
20. Li, J., & Sun, R. (2026). Study on the output performance of proton exchange membrane fuel cells with bionic leaf-like bifurcating vein channels based on fractal transport characteristics. Fuel, 406, 136934.
21. Xiao, F., Chen, T., Lan, Y., & Chen, Z. (2025). Flow field design and parameter optimization of PEMFC based on leaf vein structure. Renewable Energy, 241, 122317.